Allosteric adaptation in the stator complex rescues bacterial motility in Exb/Mot chimeras.

Authors

Pietro Ridone[1], Matthew A. B. Baker[1].

[1]School of Biotechnology and Biomolecular Sciences, UNSW Sydney, Australia.

Abstract

Powered by ion transport across the cell membrane, conserved ion-powered rotary motors (IRMs) drive bacterial motility by generating torque on the rotor of the bacterial flagellar motor. Homologous heteroheptameric IRMs have been structurally characterized in ion pumps such as Tol/Ton/Exb/Gld, and most recently in phage defense systems such as Zor. Functional stator complexes synthesized from chimeras of PomB/MotB (PotB) have been used to slow flagellar rotation via reduced external sodium concentration. Such chimeras are highly sensitive to the location of the cut-site and thus far have been arbitrarily designed. To date, no chimeras have been constructed using interchange of components from Tol/Ton/Exb/Gld and other ion powered motors with more distant homology.

Here we synthesised chimeras of MotAB, PomAPotB and ExbBD to assess their capacity for cross-compatibility. We obtained motile B-unit chimeric stator complexes whose motility was further optimised by directed evolution. Whole genome sequencing of these revealed epistatic adaptations in the A-subunit and at the peptidoglycan binding domain of the B-unit could improve motility. Overall, our work highlights the role of allostery and the challenges associated with rational design of chimeric IRMs.

Importance

Ion-powered rotary motors (IRMs) underpin the rotation of nature's oldest wheel, the flagellar motor. Indeed, they themselves appear to rotate to drive flagellar motor and may be the oldest molecular wheel. Recent structures have shown this complex drives ion pumping and even phage defence and thus appears to be a fundamental module in bionanotechnology with diverse biological utility where electrical energy can be coupled to rotational force to execute work.

Here we attempted to rationally design chimeric 'Frankenstein' IRMs to explore the cross-compatibility of these ancient motors, to try to better understand what a common ancestor may have looked like, as well as to explore possibilities to engineer this fundamental component of bionanotechnology for future application.

Introduction

Many bacteria swim propelled by the rotation of flagella to navigate themselves to better conditions. The rotation of these flagella is powered by ion-powered rotary ion-pumps known as stators[1–3]. Recent structural characterization of the proton powered stators revealed that the stators are heteroheptamers ($MotA_5MotB_2$), and this has now been observed in sodium powered stators (PomA5PomB2[3]), in ion pumps (GldM5GldN2[4], ExbB5ExbD2[5,6]) and most recently in phage defense systems (ZorA5ZorB2[7]). These ion-powered rotary machines (IRMs)[8] have highly diverse downstream functions, among which one is an essential gene for bacterial motility (*motAB*). Such high structural conservation across complexes implies a common origin: IRMs represent a key molecular complex with an origin at least as ancient as flagellar motility[9,10]. As such there is significant interest in understanding what the structure and function of a potential common ancestor might be.

The flagellar motor itself is highly modular (Fig.1). This is routinely defined at one hierarchy as the filament, hook and basal body[11], a classification which ignores the IRMs as a module themselves. We consider submodules of the motor to be identifiable domains that have a specific function: in the case of the stator-complex, this is commonly defined for the central B-unit as the transmembrane (TM) domain, the linker, and the peptidoglycan binding domain (PGB, in gram negative strains such as *E. coli*). As more structural information becomes available, it is also possible to clearly identify pore-facing, rotor-interacting, and lipid-facing domains in the pentameric A-unit[12–14].

Chimeric work in the stator complex is not new: the first Mot/Pom chimeras were designed in the early 1990s with the target of generating a sodium-powered chimera that was functional in *E. coli* [15]. Mutagenesis and protein engineering work exploring the role of the plug and linker in light of new structures continues[16–20], as well as efforts to reconstruct an ancestral stator to explore origins and divergence[13,21]. However, to our knowledge attempts to combine homologous A5B2 pumps coupled to non-flagellar function with existing stator components have not been attempted.

In this work we seek to explore the capacity for protein engineering of such functional pump-stator protein chimeras. We explore compatibility of submodules of IRMs and test these for their capacity to restore motility in stator-deleted bacterial strains. We show the capacity of the overall flagellar complex to rescue motility through epistatic mutations far from chimeric interfaces, belying the complex integration of submodules across the complex. Through doing so, we explore the limits of function as well as the potential for custom new functions and can determine essential protein motifs which differentiate structure and function across the IRM classes.

Results

We designed chimeras of *motA* and *exbB* (the A-subunit) and *motB exbD* (the B-subunit) by performing amino acid alignments between homologs (MAFFT) and by manual inspection of their 3D structures to select the residues connecting the chimeric portions of our constructs. We selected 4 A-subunit and 10 B-subunit constructs to clone into a plasmid vector (pBAD33) for *in vivo* testing in a stator-deleted strain (*E. coli* Δ*motAB*) (Fig.2A, 2B).

Each construct was maintained in culture on a soft agar swim plate for up to 2 weeks to allow for the isolation and propagation of up-motile populations. Out of all 14 tested constructs we isolated one *potB / exbD* variant ($PotD_{3.3}$) able to restore motility in presence of *pomA* (Fig. 2C). The plasmid carried by this motile population was extracted and re-sequenced across both stator genes to check for additional mutations contributing to the phenotype and a missense mutation (Q104P) was found in the chimeric construct $potD_{3.3}$. (SI Fig. 1). This stator B-subunit construct ($potD_{3.3}$ *Q104P*) was renamed "PotDα".

PotDα was further tested in presence of *motA* and all chimeric A-subunit constructs to check whether together they could form a functional stator (Fig. 3A, 3B). None of our *potDα* / A-subunit combinations produced swim rings within 24 hr (SI Fig. 2A) while control combinations (*motAmotB*, *motApotB* and *pomApotB*) all formed swim rings on plates and with observable swimmers at the single cell level (Fig. 3C). Thus, none of our A-subunit chimeras appeared to function in presence of any B subunit partner, whether chimeric or wild-type. Bacteria co-expressing the *mobB.v1 potDα* combination showed a slower growth phenotype when compared to *motAmotB* control (SI Fig.2B)

Swim rings of *pomApotDα* spread noticeably slower than *pomApotB*. To test for capacity to rescue motility in non-motile chimeras, we passaged subpopulations on fresh swim plates at 3-4 days intervals. After 6 passages, visible swim rings of *pomApotDα* formed within a 24-hr period (Fig. 4A). The *potDα* variant was motile not only in the presence of both *motA* and *pomA* but also when only *pomA* was present (tested in Δ*motB E. coli* RP3087, *motB* on genome *pomA* on plasmid; or *E. coli* Δ*motAB,* only *pomA* from plasmid). Plasmid re-sequencing of this variant revealed an additional mutation in the plasmid-encoded *pomA* gene (A86V). All other B-subunit constructs, which started non-motile, showed no rescue in motility after 6 passages.

We used genome-based directed evolution of motility [22] to attempt to further improve motility of our chimeric variant. We replaced the native *motAB* locus *E. coli* RP437 with the *pomApotDα* construct cloned from the plasmid (SI Fig.3A, 3B). As observed in plasmid maintained directed evolution, motility improved over several passages and mutations were found in the up-motile population (Fig. 4B). A control genomic edit using the original $potD_{3.3}$ construct (*E. coli* "PotD", SI Fig.3A), without additional mutations, did not adapt to rescue motility (SI Fig.3C). Whole-genome sequencing of members of our PotDα evolved lineage revealed a new missense mutation in the chromosomal *pomA* gene (H116Y) and additional mutations in the *flgM* and *icd* genes (Fig. 4B, SI Table 1).

To verify the effect of these stator mutations we reintroduced them into the plasmid-encoded *pomApotDα* constructs via site-directed mutagenesis and measured their effect on motility in our stator deleted strain (*E. coli* Δ*motAB*). Growth profiles of all our evolved and engineered strains showed no effect on growth when *potDα* was expressed from plasmids, while growth was inhibited when the construct was expressed from the edited locus on the chromosome (SI Fig. 4A). At the same time, we tested the effect on swim rings of the presence and absence of sodium to infer the ion-selectivity of the chimeric stator (Fig. 5A, SI Fig. 4B). Our chimera appeared to require Na^+ for effective motility and did not produce swim rings on K^+ swim plates. Motility was inhibited in presence of the Na^+-powered stator blocker Phenamil (SI Fig. 4B). Our plasmid-based validation showed that mutations in *pomA* at H116Y/A86V improved the

motility phenotype when co-expressed with *potDα* (Fig. 5B). Structurally, while the $PotD_{3.3}$ mutation Q104P was found at the N-terminal end of the PG-binding domain, both PomA mutations were located on the cytoplasmic side of the stator, proximal to the surface interacting with the rotor of the BFM (FliG, YcgR), indicating a synergistic effect to improve motility.

Discussion

We engineered 10 B-subunit chimeras with varying degrees of *exbD* content (5.3% $PotD_{3.3}$ – 16.95% $PotD_{4.2}$). Of these, the construct with the most minimal *exbD* composition (*$potD_{3.3}$*) was able to generate torque and rescue motility following subsequent adaptation with directed evolution. None of our A-subunit chimeras were functional or rescued by directed evolution, however mutations in *pomA* did improve motility further when co-expressed with *$potD_{3.3}$*, and these mutations were far from the pore, proximal to the rotor interface.

Cut-sites are critical in B-unit

It is challenging to determine why some chimeras are functional where others are not, especially considering some B-unit chimeras differed only very slightly. Chimeras that differed by only 4 residues ($PotD_{3.0}$), in non-conserved regions adjacent to the pore were unable to rescue motility. This is indicative of the general challenge of rational design and the need to consider carefully cut-sites and attempt multiple variants simultaneously (towards irrational design) to improve throughput. Single amino acid replacements within the TM domain of *Ec*MotB are likely to disrupt motility even when conservative[23].

Preservation of pore proximal A-B interface does not guarantee function.

To date, no functional A-unit chimeras have been made, either from Mot/Pom complexes or across the ion powered rotary motors more widely. Here we matched A-B interfaces across the pore, ie, across TM region of *Ec*MotB (residues I28-W45) and TM3/4 in *Ec*MotA (residues N139-N250) (SI Fig. 5A, 5B). Despite this, none were functional in driving torque-generation and motility. One combination of chimeric variants aimed at reconstituting a complete ExbBD-like pore (*mobB.v1 potDα*) caused growth-delaying effects when expressed, suggesting that it may have been able to pass ions without coupling conduction to torque generation (SI Fig.5C, 5D). We have not demonstrated complete folding or expression of our A-unit such as via Western blot or RT-PCR. Allowing for this, our results indicate that regions outside the pore are important in improving edits made at the site of the pore. However, when the lipid and rotor interfaces were preserved by using a single A-subunit with known functional domains in these locations (*mobB.v1*, *mobB.v2* and *potA*, Fig.2A), these chimeras were still non motile.

Allosteric and epistatic mutations further improve motility in partially functional stators.

Motility was rescued in *$potD_{3.3}$* via a point mutation at a residue far from the pore, Q104. Subsequent mutations that improved motility were observed near a known FliG interaction site of the A-subunit (PomA) at A86 and H116. Regions far from the pore can not only affect function but also repair edits at the pore to enable function. Mutations far from the pore have been shown to affect phenamil binding and resistance[24], putatively through stabilization of stator binding allowing a dysfunctional stator to persist in being engaged with the rotor for longer. It is possible here that stabilizing the PG-binding of the stator complex would enable motility driven by a partially functional stator. Such allosteric interactions

undermine attempts to rationally design proteins through edits at only a single functional site. Methods exist to examine allosteric networks across proteins which can help these attempts [25–27].

Chimeric testing occurs in single hosts with different motors and membrane environments.

We sought to design chimeras that preserved ion conduction, torque generation and mechanosensitivity and approached this via engineering conservative chimeras centered around the pore. The stator complex has multiple functions, executed by specific domains of the complex that are either pore facing (TM3-4 residues N139-N250 in *Ec*MotA), rotor-facing (residues L81-M138) or PG binding (residues N102-L288 in *Ec*MotB). Not only must the stator complex sense force to activate and transduce chemical potential into torque, but it must also interact with the rotor to couple torque to filament rotation, and the rotor is itself a large molecular complex with multiple functions including switching chemotaxis as well as rotation. All chimeras in our work were only tested in an *E. coli* chassis. Motors in different species have different protein and membrane composition, different sizes, as well as different stator dynamics[28–30]. Thus it is possible our stators are functional but require rotor and membrane environments that are better matched to their chimeric pores. Single molecule *in vitro* bilayer measurements with energetic controls could provide control of lipid composition and a platform to better assay the function of the protein in isolation to better elucidate which submodules of the motor retain partial functionality, whereas in our motility assays we are only able to test overall function as presence or absence of motility.

Directed and experimental evolution improves function rapidly.

As in our previous work, during iterative swim plating we observed mutants that upregulate filament expression[22,31]. Both our plasmid-based and genomic directed evolution generated convergent results. Mutations far from the pore site rescued function quickly in the time-frame of days. These screens allow us to explore epistatic interactions that rescue motility, such as non-pore residues improving function in differing environments. However, a simple swim plate does confound growth, motility and chemotaxis, so does not target mutations directly to the capacity for the stator complex to be ion selective or generate torque[22]. Nevertheless, we do see mutations that repair edits and improve performance on swim plates and can correlate these to subsequent biophysical measurements, such as tethered cell assays[32–34].

More specific screens that directly target motility[35] or cell energetics could be applied to select for mutations that affect the function of specific submodules of the stator complex. Likewise, *in vitro* methods could better discern subtle variations in arising phenotypes[18,36]. Improved preparation of combinatoric libraries using newer approaches in synthetic biology could improve throughput[37–40]. Here we utilized medium throughput biological methods that are still able to screen one-in-a-million up-motile variants[24]. Future high-throughput screens will require automated colony passaging by liquid-handling or colony-picking robots which would allow the exploration of new mutations that rescue or alter function from more varied starting points, across larger combinatoric libraries of IRMs.

Conclusions

Our work shows that even with as few as 12 amino acid substitutions, cut-site location and chimeric design is challenging and requires high-throughput approaches to succeed. Recent structural characterization of structural homologues of the stator complex, including Zorya, has shown the diversity of biological applications where IRMs can transduce energy from ion gradients to mechanical work. A common

ancestor of these IRMs which would shed light on the origin of the stator complex, as well as other complexes, and this may be a key innovation of function in early life.

Construction of chimeras exchanging components between extant homologues does not necessarily inform the structure and function of this common ancestor, but it does allow us to examine what are the core elements of these complexes, as well as understand which modules are interchangeable and which are not. This can inform the order of events under which the stator complex arose and diversified and inform parsimony approaches to loss and gain of function in subsequent adaptation. Further studies with new methods in statistical and structural phylogenetics are required to target ancestors of the stator complex for characterization both structurally and biophysically.

Materials and Methods

E. coli strains, plasmids, and culture media

Synthetic stator chimeras were tested in stator-deleted derivative strains of *E. coli* RP437, either *E. coli* Δ*motB* (RP3087 (ref) or *E. coli* Δ*motAB* (SI Fig. 3). For genomic edits, *E. coli* RP437 was used as the parent strain[41,42] to with the native *motAB* locus edited using No-SCAR methods, as previously [32]. The pSHU1234 (pBAD33 backbone, Cm+) plasmid encoding *pomA* and *potB* [24] was used as the vector to clone and express all chimeric constructs.

Chimeric constructs were designed *in silico* and synthesized by Integrated DNA Technologies (IDT) as gene fragments (gBlocks). Chimeras were cloned in plasmid pSHU1234 using restriction digestion with NdeI and PstI (New England Biolabs). Plasmids carrying chimeric constructs were used as templates to generate the double-stranded donor DNA used to replace the *motA* and *motB* gene on the RP437 chromosome with *pomA* and *potD* variants, respectively (see Scar-less editing).

Point mutations in plasmids were generated using the QuikChange technique. Bicistronic plasmids expressing both A and B stator subunits were converted to single-gene plasmids expressing only the B-subunit via inverse deletion PCR. Single-construct plasmids expressing A-subunits were constructed via restriction digestion (NdeI and PstI, New England Biolabs) and ligation using pBAD24 (Amp+) as a plasmid backbone.

Cloned constructs were confirmed by Sanger sequencing (Ramaciotti Centre for Genomics, Kensington).

Liquid cell culturing was done using LB broth (NaCl or KCl, 0.5% yeast extract (70161, Sigma-Aldrich), and 1% Bacto tryptone). Cells were cultured on agar plates composed of LB broth and 1% Bacto agar (BD Biosciences, USA). Swim plate cultures were performed on the same substrates adjusted for agar content (0.25% Bacto agar). Inhibition of Na+-dependent motility was performed using 100 µM phenamil methanesulfonate (P203, Sigma-Aldrich).

Scar-less editing of *E. coli* with Cas9-assisted recombineering

This procedure was adapted from the no-SCAR method[43]. The target strain to be edited (E. coli RP437) was sequentially transformed first with the pKD-sgRNA-3'MotA (Sm+) plasmid, encoding a single guide RNA (sgRNA) sequence directed at the 3' end of *motA*, and then with the pCas9cr4 (Cm+) plasmid to yield a parent strain harboring both plasmids. The overlap extension PCR technique[44] was used to assemble linear double-stranded DNA (dsDNA) molecules using two (knock-out) or three (knock-in) starting dsDNA fragments. The resulting donor DNA was electroporated in the plasmid-bearing host, and the successfully

edited clones were selected via colony PCR and Sanger sequencing of the *motAB* locus. A list of oligonucleotide primers and synthetic gene fragments (gBlocks) used in this work is provided in Supplementary Table 2.

Free-swimming assay preparation and analysis

Free-swimming cells were grown overnight in tryptone buffer (TB: tryptone, 85 mM NaCl) at 30°C to OD600 of ~0.5, diluted 100x in TB and loaded for imaging in a tunnel slide. A custom LabVIEW software was used as previously[21,24,32] reported to estimate the speed of swimming cells. Time-lapse videos were collected using a camera (Chameleon3 CM3, Point Grey Research) recording 20-s-long videos at 20 frames/s. Visualization of the data was performed using GraphPad Prism 8.

Sequencing and genomics

WGS of *E. coli* strains was performed using a MiSeq 2 × 150–base pair (bp) chip on an Illumina sequencing platform. Sequencing was carried out at the Ramaciotti Centre for Genomics, Kensington and delivered as demultiplexed fastQ files (quality control: >80% bases higher than Q30 at 2 × 150 bp). The SNP calling and analysis were performed using Snippy[45–47]. The short reads from sequencing were aligned to the MG1655 reference *E. coli* genome (GenBank: U00096.2) and an *E. coli* RP437 (GenBank: CP083410.1) as previously [22]. A summary of all single nucleotide polymorphisms (SNPs) detected in this study is provided in Supplementary Table 2.

Structural modelling

Models of stator monomers and heptameric complexes was performed using AlphaFold2 on Galaxy.au, using the Australian Alphafold Service (AAS). The software was run in multimer mode using FASTA files as input[48,49]. Models were visualized and prepared for figures using PyMOL.

Acknowledgements

M.A.B.B. acknowledges funding support from a Scientia Fellowship from UNSW, Human Frontiers Science Program Project Grant No. RGY0072/21 and U.S. Navy Office of Naval Research Research Grant No. N62909-22-1-2051.

References

1. Santiveri, M., Roa-Eguiara, A., Kühne, C., Wadhwa, N., Hu, H., Berg, H.C., Erhardt, M., and Taylor, N.M.I. (2020). Structure and Function of Stator Units of the Bacterial Flagellar Motor. Cell *183*, 244-257.e16. 10.1016/j.cell.2020.08.016.

2. Deme, J.C., Johnson, S., Vickery, O., Aron, A., Monkhouse, H., Griffiths, T., James, R.H., Berks, B.C., Coulton, J.W., Stansfeld, P.J., et al. (2020). Structures of the stator complex that drives rotation of the bacterial flagellum. Nat Microbiol *5*, 1553–1564. 10.1038/s41564-020-0788-8.

3. Hu, H., Popp, P.F., Santiveri, M., Roa-Eguiara, A., Yan, Y., Martin, F.J.O., Liu, Z., Wadhwa, N., Wang, Y., Erhardt, M., et al. (2023). Ion selectivity and rotor coupling of the Vibrio flagellar sodium-driven stator unit. Nat Commun *14*, 4411. 10.1038/s41467-023-39899-z.

4. Hennell James, R., Deme, J.C., Kjær, A., Alcock, F., Silale, A., Lauber, F., Johnson, S., Berks, B.C., and Lea, S.M. (2021). Structure and mechanism of the proton-driven motor that powers type 9 secretion and gliding motility. Nature Microbiology *6*, 221–233. 10.1038/s41564-020-00823-6.

5. Celia, H., Noinaj, N., and Buchanan, S.K. (2020). Structure and Stoichiometry of the Ton Molecular Motor. Int J Mol Sci *21*, 375. 10.3390/ijms21020375.

6. Maki-Yonekura, S., Matsuoka, R., Yamashita, Y., Shimizu, H., Tanaka, M., Iwabuki, F., and Yonekura, K. (2018). Hexameric and pentameric complexes of the ExbBD energizer in the Ton system. eLife *7*, e35419. 10.7554/eLife.35419.

7. Hu, H., Hughes, T.C.D., Popp, P.F., Roa-Eguiara, A., Martin, F.J.O., Rutbeek, N.R., Hendriks, I.A., Payne, L.J., Yan, Y., Sousa, V.K. de, et al. (2023). Structure and mechanism of Zorya anti-phage defense system. Preprint at bioRxiv, 10.1101/2023.12.18.572097 10.1101/2023.12.18.572097.

8. Nandel, V., Scadden, J., and Baker, M.A.B. (2023). Ion-Powered Rotary Motors: Where Did They Come from and Where They Are Going? International Journal of Molecular Sciences *24*, 10601. 10.3390/ijms241310601.

9. Beeby, M., Ferreira, J.L., Tripp, P., Albers, S.-V., and Mitchell, D.R. (2020). Propulsive nanomachines: the convergent evolution of archaella, flagella and cilia. FEMS Microbiology Reviews *44*, 253–304. 10.1093/femsre/fuaa006.

10. Miyata, M., Robinson, R.C., Uyeda, T.Q.P., Fukumori, Y., Fukushima, S., Haruta, S., Homma, M., Inaba, K., Ito, M., Kaito, C., et al. (2020). Tree of motility – A proposed history of motility systems in the tree of life. Genes to Cells *25*, 6–21. 10.1111/gtc.12737.

11. Armitage, J.P., and Berry, R.M. (2020). Assembly and Dynamics of the Bacterial Flagellum. Annu Rev Microbiol *74*, 181–200. 10.1146/annurev-micro-090816-093411.

12. Chang, Y., Zhang, K., Carroll, B.L., Zhao, X., Charon, N.W., Norris, S.J., Motaleb, M.A., Li, C., and Liu, J. (2020). Molecular mechanism for rotational switching of the bacterial flagellar motor. Nat Struct Mol Biol *27*, 1041–1047. 10.1038/s41594-020-0497-2.

13. Islam, M.I., Ridone, P., Lin, A., Michie, K.A., Matzke, N.J., Hochberg, G., and Baker, M.A.B. (2023). Ancestral reconstruction of the MotA stator subunit reveals that conserved residues far from the pore are required to drive flagellar motility. microLife *4*, uqad011. 10.1093/femsml/uqad011.

14. Johnson, S., Deme, J.C., Furlong, E.J., Caesar, J.J.E., Chevance, F.F.V., Hughes, K.T., and Lea, S.M. (2024). Structural basis of directional switching by the bacterial flagellum. Nat Microbiol, 1–11. 10.1038/s41564-024-01630-z.

15. Asai, Y., Yakushi, T., Kawagishi, I., and Homma, M. (2003). Ion-coupling Determinants of Na+-driven and H+-driven Flagellar Motors. Journal of Molecular Biology *327*, 453–463. {10.1016/S0022-2836(03)00096-2}.

16. Kojima, S., Takao, M., Almira, G., Kawahara, I., Sakuma, M., Homma, M., Kojima, C., and Imada, K. (2018). The helix rearrangement in the periplasmic domain of the flagellar stator B subunit activates peptidoglycan binding and ion influx. Structure *26*, 590-598.e5. 10.1016/j.str.2018.02.016.

17. Miyamura, Y., Nishikino, T., Koiwa, H., Homma, M., and Kojima, S. (2024). Roles of linker region flanked by transmembrane and peptidoglycan binding region of PomB in energy conversion of the Vibrio flagellar motor. Genes to Cells *n/a*. 10.1111/gtc.13102.

18. Nishikino, T., Iwatsuki, H., Mino, T., Kojima, S., and Homma, M. (2020). Characterization of PomA periplasmic loop and sodium ion entering in stator complex of sodium-driven flagellar motor. The Journal of Biochemistry *167*, 389–398. 10.1093/jb/mvz102.

19. Takekawa, N., Isumi, M., Terashima, H., Zhu, S., Nishino, Y., Sakuma, M., Kojima, S., Homma, M., and Imada, K. (2019). Structure of Vibrio FliL, a New Stomatin-like Protein That Assists the Bacterial Flagellar Motor Function. MBio *10*. 10.1128/mBio.00292-19.

20. Zhu, S., Nishikino, T., Takekawa, N., Terashima, H., Kojima, S., Imada, K., Homma, M., and Liu, J. (2020). In Situ Structure of the Vibrio Polar Flagellum Reveals a Distinct Outer Membrane Complex and Its Specific Interaction with the Stator. Journal of Bacteriology *202*, 10.1128/jb.00592-19. 10.1128/jb.00592-19.

21. Islam, M.I., Lin, A., Lai, Y.-W., Matzke, N.J., and Baker, M.A.B. (2020). Ancestral Sequence Reconstructions of MotB Are Proton-Motile and Require MotA for Motility. Front. Microbiol. *11*. 10.3389/fmicb.2020.625837.

22. Ridone, P., Ishida, T., Lin, A., Humphreys, D.T., Giannoulatou, E., Sowa, Y., and Baker, M.A.B. (2022). The rapid evolution of flagellar ion selectivity in experimental populations of E. coli. Science Advances *8*, eabq2492. 10.1126/sciadv.abq2492.

23. Ridone, P., Winter, D.L., and Baker, M.A.B. (2023). Tuning the stator subunit of the flagellar motor with coiled-coil engineering. Protein Science *32*, e4811. 10.1002/pro.4811.

24. Ishida, T., Ito, R., Clark, J., Matzke, N.J., Sowa, Y., and Baker, M.A.B. (2019). Sodium-powered stators of the bacterial flagellar motor can generate torque in the presence of phenamil with mutations near the peptidoglycan-binding region. Molecular Microbiology *111*, 1689–1699. https://doi.org/10.1111/mmi.14246.

25. Gouridis, G., Muthahari, Y.A., de Boer, M., Griffith, D.A., Tsirigotaki, A., Tassis, K., Zijlstra, N., Xu, R., Eleftheriadis, N., Sugijo, Y., et al. (2021). Structural dynamics in the evolution of a bilobed protein scaffold. Proceedings of the National Academy of Sciences *118*, e2026165118. 10.1073/pnas.2026165118.

26. Salinas, V.H., and Ranganathan, R. (2018). Coevolution-based inference of amino acid interactions underlying protein function. Elife *7*, e34300. 10.7554/eLife.34300.

27. Teşileanu, T., Colwell, L.J., and Leibler, S. (2015). Protein sectors: statistical coupling analysis versus conservation. PLoS Comput Biol *11*, e1004091. 10.1371/journal.pcbi.1004091.

28. Chaban, B., Coleman, I., and Beeby, M. (2018). Evolution of higher torque in *Campylobacter*-type bacterial flagellar motors. Sci Rep *8*, 97. 10.1038/s41598-017-18115-1.

29. Chen, S., Beeby, M., Murphy, G.E., Leadbetter, J.R., Hendrixson, D.R., Briegel, A., Li, Z., Shi, J., Tocheva, E.I., Müller, A., et al. (2011). Structural diversity of bacterial flagellar motors. EMBO J. *30*, 2972–2981. 10.1038/emboj.2011.186.

30. Nord, A.L., Gachon, E., Perez-Carrasco, R., Nirody, J.A., Barducci, A., Berry, R.M., and Pedaci, F. (2017). Catch bond drives stator mechanosensitivity in the bacterial flagellar motor. Proc Natl Acad Sci U S A *114*, 12952–12957. 10.1073/pnas.1716002114.

31. Ni, B., Colin, R., Link, H., Endres, R.G., and Sourjik, V. (2020). Growth-rate dependent resource investment in bacterial motile behavior quantitatively follows potential benefit of chemotaxis. PNAS *117*, 595–601. 10.1073/pnas.1910849117.

32. Islam, M.I., Bae, J.H., Ishida, T., Ridone, P., Lin, J., Kelso, M.J., Sowa, Y., Buckley, B.J., and Baker, M. a. B. (2021). Novel Amiloride Derivatives That Inhibit Bacterial Motility across Multiple Strains and Stator Types. J Bacteriol *203*, e0036721. 10.1128/JB.00367-21.

33. Kinosita, Y., Ishida, T., Yoshida, M., Ito, R., Morimoto, Y.V., Goto, K., Berry, R.M., Nishizaka, T., and Sowa, Y. (2020). Distinct chemotactic behavior in the original Escherichia coli K-12 depending on forward-and-backward swimming, not on run-tumble movements. Sci Rep *10*, 15887. 10.1038/s41598-020-72429-1.

34. Nishiyama, M., and Kojima, S. (2012). Bacterial Motility Measured by a Miniature Chamber for High-Pressure Microscopy. International Journal of Molecular Sciences *13*, 9225–9239. 10.3390/ijms13079225.

35. Gurung, J.P., Navvab Kashani, M., Agarwal, S., Peralta, G., Gel, M., and Baker, M.A.B. (2021). Separation and enrichment of sodium-motile bacteria using cost-effective microfluidics. Biomicrofluidics *15*, 034108. 10.1063/5.0046941.

36. Lin, T.-S., Zhu, S., Kojima, S., Homma, M., and Lo, C.-J. (2018). FliL association with flagellar stator in the sodium-driven Vibrio motor characterized by the fluorescent microscopy. Scientific Reports *8*, 11172. 10.1038/s41598-018-29447-x.

37. Currin, A., Parker, S., Robinson, C.J., Takano, E., Scrutton, N.S., and Breitling, R. (2021). The evolving art of creating genetic diversity: From directed evolution to synthetic biology. Biotechnol Adv *50*, 107762. 10.1016/j.biotechadv.2021.107762.

38. Liu, L., Huang, Y., and Wang, H.H. (2023). Fast and efficient template-mediated synthesis of genetic variants. Nat Methods *20*, 841–848. 10.1038/s41592-023-01868-1.

39. Marsischky, G., and LaBaer, J. (2004). Many Paths to Many Clones: A Comparative Look at High-Throughput Cloning Methods. Genome Res. *14*, 2020–2028. 10.1101/gr.2528804.

40. Quaglia, D., Ebert, M.C.C.J.C., Mugford, P.F., and Pelletier, J.N. (2017). Enzyme engineering: A synthetic biology approach for more effective library generation and automated high-throughput screening. PLOS ONE *12*, e0171741. 10.1371/journal.pone.0171741.

41. Block, S.M., Blair, D.F., and Berg, H.C. (1989). Compliance of bacterial flagella measured with optical tweezers. Nature *338*, 514–518. 10.1038/338514a0.

42. Parkinson, J.S. (1978). Complementation analysis and deletion mapping of Escherichia coli mutants defective in chemotaxis. J Bacteriol *135*, 45–53.

43. Reisch, C.R., and Prather, K.L.J. (2015). The no-SCAR (Scarless Cas9 Assisted Recombineering) system for genome editing in Escherichia coli. Sci Rep *5*, 15096. 10.1038/srep15096.

44. Higuchi, R., Krummel, B., and Saiki, R.K. (1988). A general method of in vitro preparation and specific mutagenesis of DNA fragments: study of protein and DNA interactions. Nucleic Acids Res *16*, 7351–7367.

45. Bush, S.J., Foster, D., Eyre, D.W., Clark, E.L., De Maio, N., Shaw, L.P., Stoesser, N., Peto, T.E.A., Crook, D.W., and Walker, A.S. (2020). Genomic diversity affects the accuracy of bacterial single-nucleotide polymorphism-calling pipelines. Gigascience *9*, giaa007. 10.1093/gigascience/giaa007.

46. Pertea, M., Pertea, G.M., Antonescu, C.M., Chang, T.-C., Mendell, J.T., and Salzberg, S.L. (2015). StringTie enables improved reconstruction of a transcriptome from RNA-seq reads. Nat Biotechnol *33*, 290–295. 10.1038/nbt.3122.

47. Seemann, T. (2024). tseemann/snippy.

48. Evans, R., O'Neill, M., Pritzel, A., Antropova, N., Senior, A., Green, T., Žídek, A., Bates, R., Blackwell, S., Yim, J., et al. (2022). Protein complex prediction with AlphaFold-Multimer. Preprint at bioRxiv, 10.1101/2021.10.04.463034 10.1101/2021.10.04.463034.

49. Jumper, J., Evans, R., Pritzel, A., Green, T., Figurnov, M., Ronneberger, O., Tunyasuvunakool, K., Bates, R., Žídek, A., Potapenko, A., et al. (2021). Highly accurate protein structure prediction with AlphaFold. Nature *596*, 583–589. 10.1038/s41586-021-03819-2.

Figures

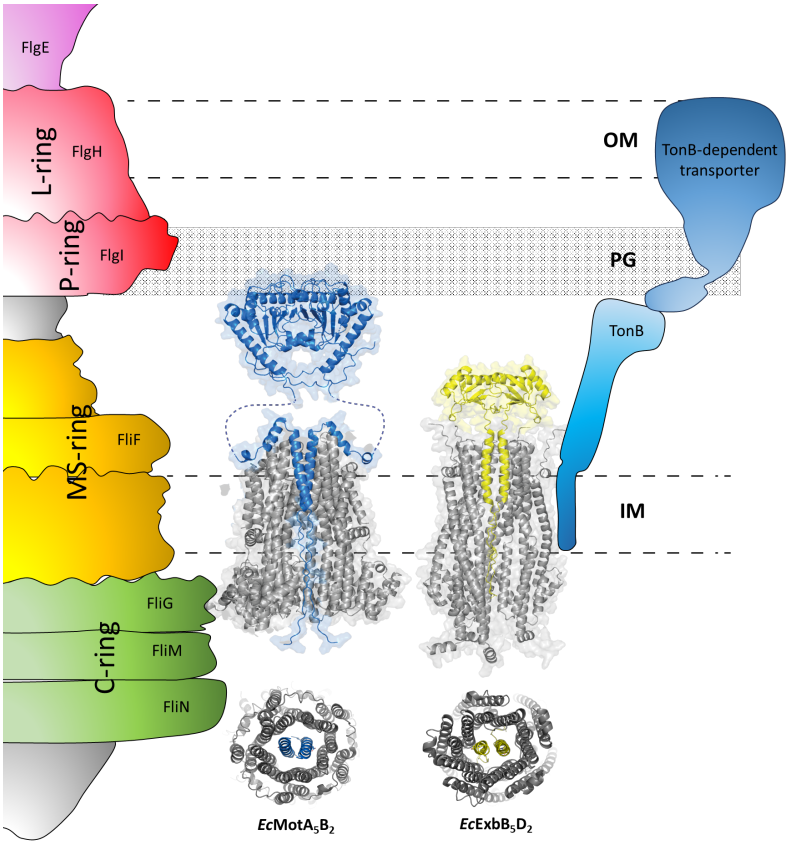

Figure 1. Overview of *E. coli* MotAB and ExbBD complexes.

The Bacterial Flagellar Motor and the TonB-dependent siderophore uptake system of *E.coli* are powered, respectively, by two homologous heptameric systems, the MotA MotB and the ExbB ExbD complexes. These two transmembrane systems share their general architecture, subunit stoichiometry and functional features, as both depend on interaction with the peptidoglycan (PG) layer and the presence of an ion-motive force (IMF) to operate. The MotAB complex interacts with FliG at the cytoplasmic interface of the basal body of the BFM (left) while the ExbBD complex is thought to interact with the TM domain of TonB at the plasma membrane.

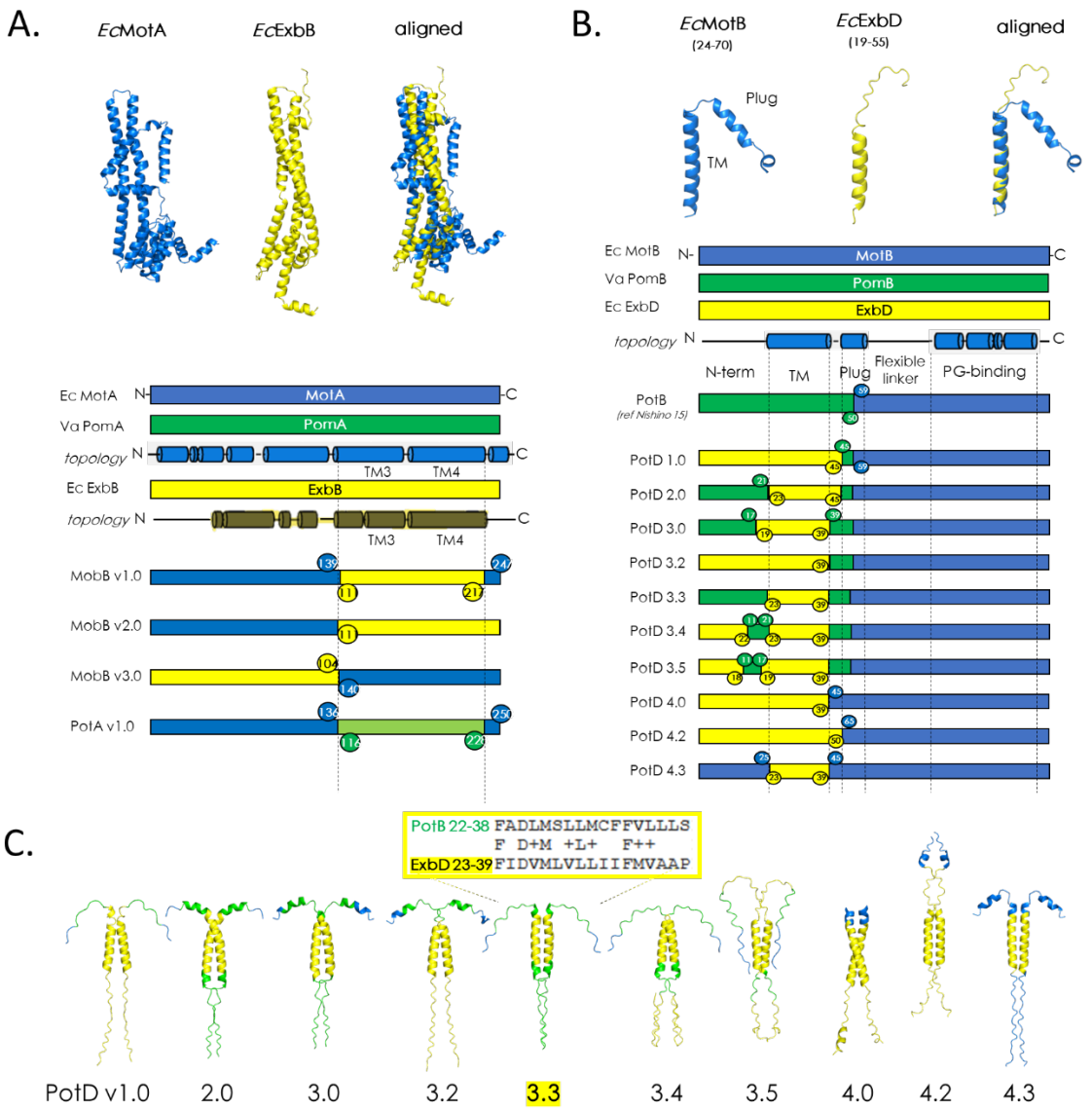

Figure 2. Design of Chimeric Exb/Mot complexes.

Chimeric constructs of MotA/PomA/ExbB (A) and MotB/PotB/ExbD (B) were designed based on the topology of each subunit. The constructs show in (A) were spliced at the junction between the N-terminal section of the protein and the more conserved TM3/4 domains. Similarly, the constructs in (B) were spliced at various points within the *N-terminal*, *TM* and *Plug* domains of the protein while retaining the *flexible linker* and *PG-binding* domains of MotA unchanged, based on a previously developed MotB/PomB chimera (PotB, Nishino et al. 2015). The amino acid residues at the junction points of each construct are indicated on each bar diagram and color-coded according to their identity (blue: MotA and MotB, green: PomA and PomB, yellow: ExbB and ExbD). C) Alphafold2 dimeric models of B-subunit chimeras (PotD variants) shown in **B** (with only *N-terminal*, *TM* and *Plug* domains shown), coloured according to their original. PotD v3.3 is highlighted in yellow, and its degree of conservation compared to PotB is shown in the box above the model.

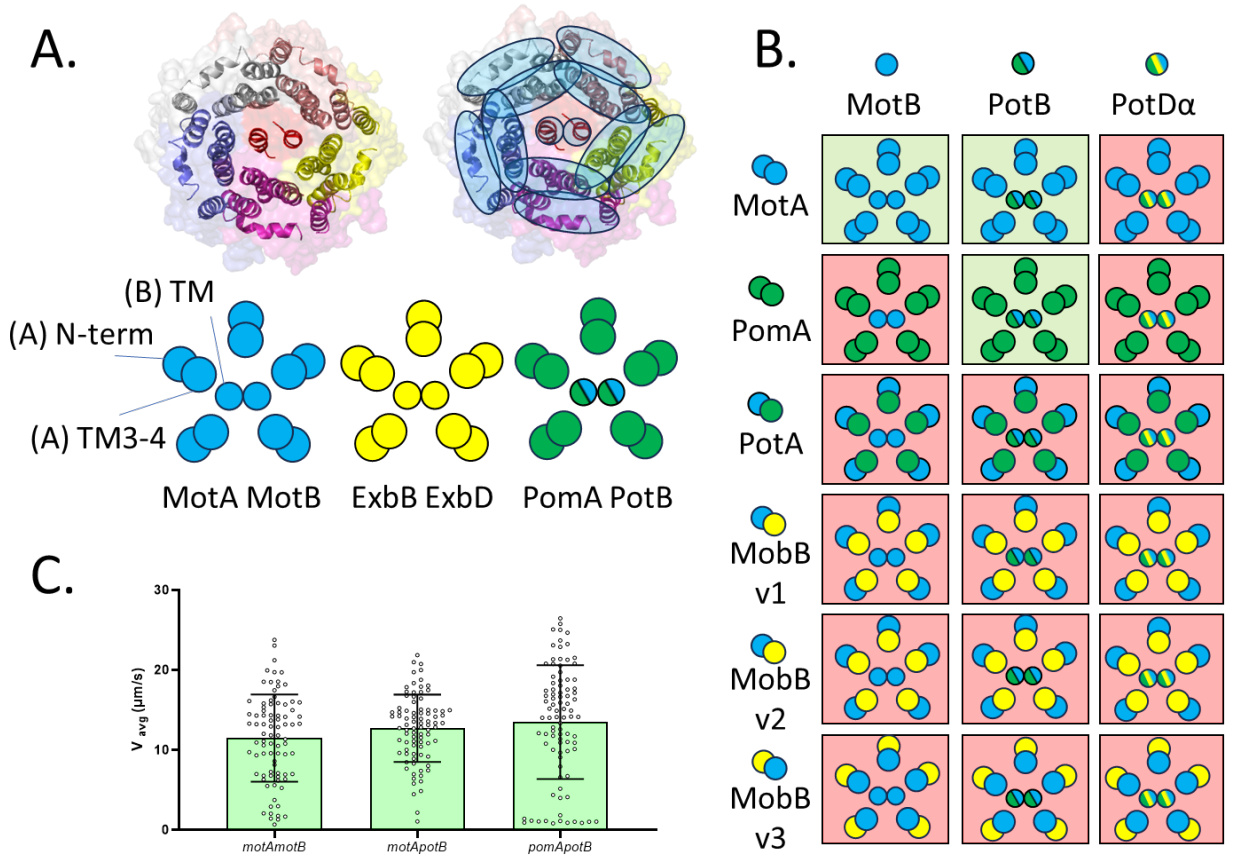

Figure 3. Functional characterization of A-B chimeric interfaces.

(A) Section of the stator complex A-B interface viewed from the periplasmic side. Monomers of MotA, shown in different colors, and blue ovals highlight the pore-facing (interior) and lipid-facing (exterior) residues of the complex. Circular diagrams are used to illustrate the intended arrangement of each protein subdomain in the chimeras tested for their ability to rescue motility. (B) Summary of all motility tests performed in stator-deleted *E. coli* co-transformed with plasmids bearing an A-subunit construct (rows) and a B-subunit construct (columns). The background color of each box indicates a motile (green) or non-motile (red) phenotype. Each A-B combination is schematically represented using the symbology shown in A. (C) Single cell free swimming cell velocity measurements for motile stator complexes shown in (B), expressed from plasmid in *E. coli* Δ*motAB* (N = 84 (MotAMotB), 86 (MotAPotB) and 90 (PomAPotB) cells).

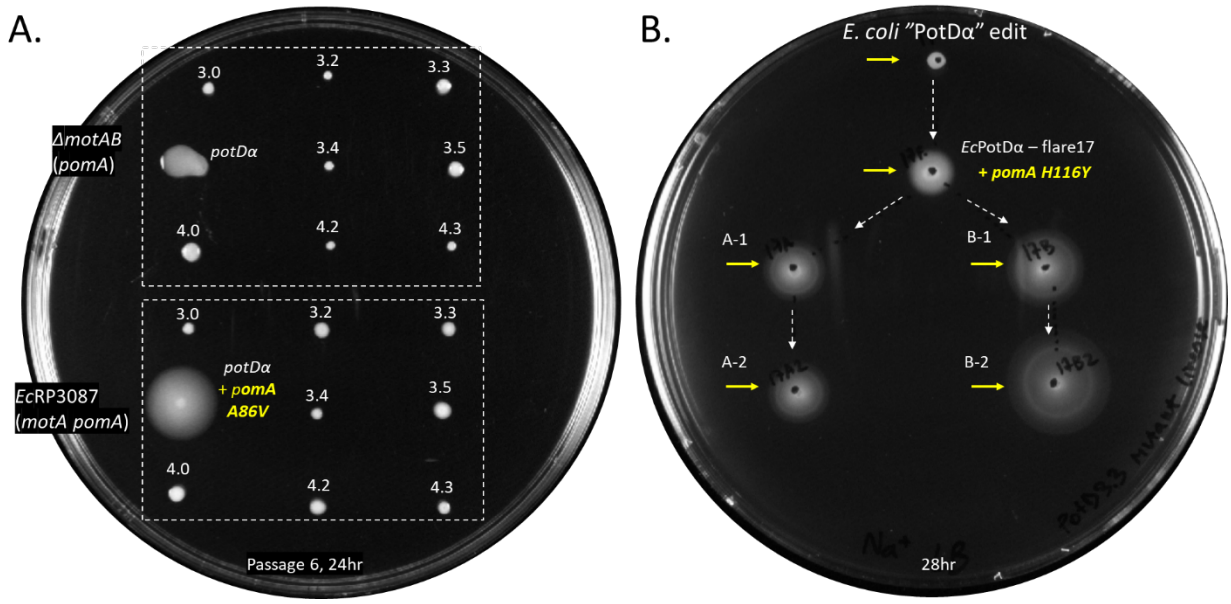

Figure 4. Optimization of motility via directed evolution of stator chimeras.

(A) Motile phenotype of *ΔmotAB* (top) and RP3087 (*ΔmotB,* bottom) *E. coli* strains expressing B-subunit chimeras after 24 hr of culture on soft-agar plates (10 cm diameter). Clones were propagated on swim agar for 6 passages prior to the experiment shown here. Yellow labels indicate motile variants and any mutation found in their construct-bearing plasmids after resequencing. The upmotile *pomA* A86V mutation found in ΔmotB *E. coli* RP3087 carrying PomAPotDα on plasmid is highlighted. (B) Motile phenotype of a synthetic lineage edited to replace the native *motA motB* locus of *E. coli* RP437 with *pomApotD*$_{3.3}$ Q104P (*E. coli* "PotDα") after 28 hr of culture on 0.3% soft agar. The original edited strain is shown at the top of the plate. Clones descending from repeated passages of motile subpopulations of the edited strain are shown below to recapitulate lineages A and B, linked by dotted arrows. Whole-genome sequencing of all six lineage members revealed the presence of the *pomA H116Y* mutation in all descendants of the original edit. A complete list of mutations found from WGS of all lineage members is reported in Supplementary Table 1.

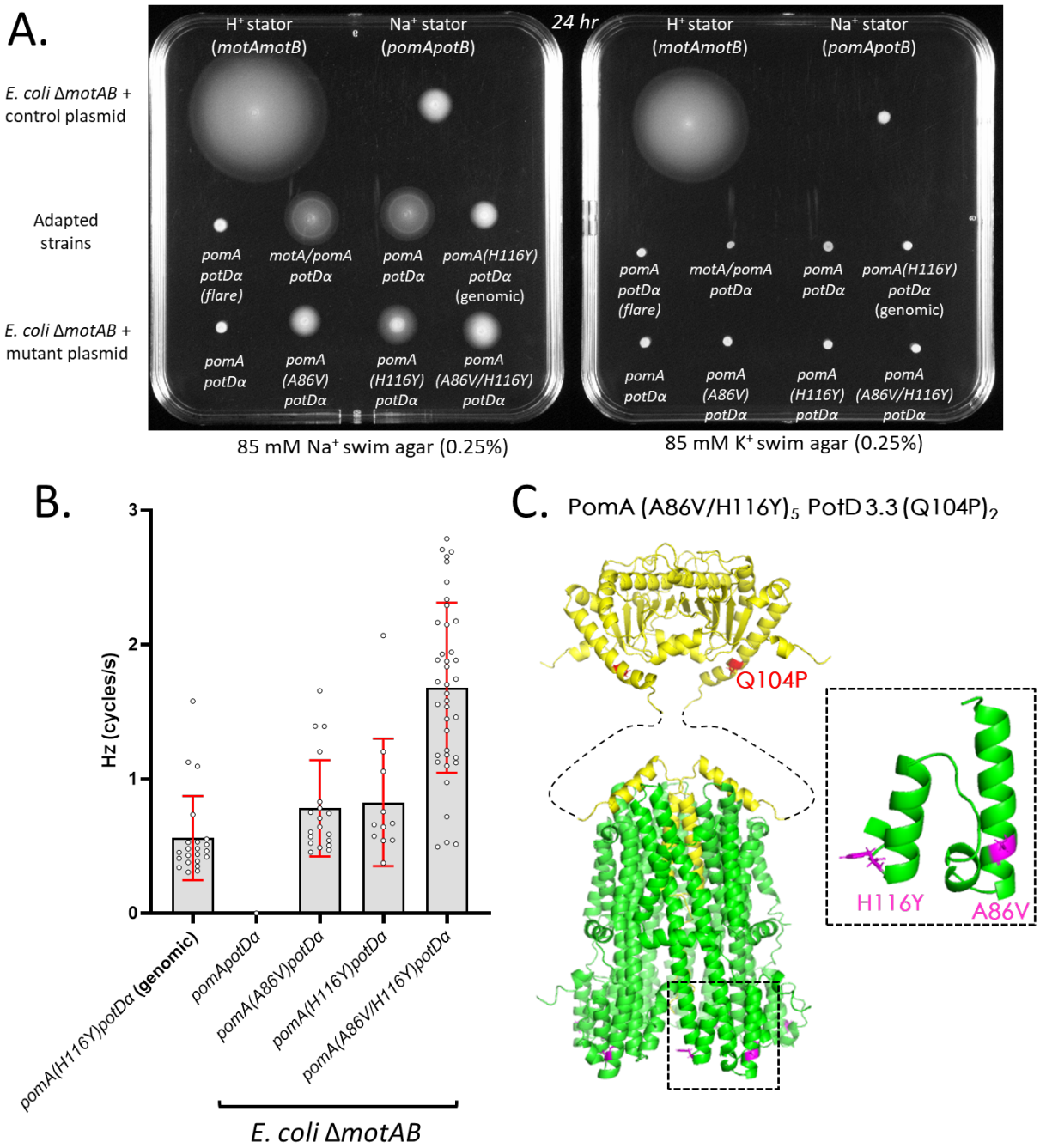

Figure 5. Functional chimeras require Sodium for function.

(A) Comparison of motile phenotypes of *E. coli* strains. Stator-deleted Δ*motAB E. coli* harbouring a proton-powered (MotAMotB) or sodium-powered (PomA/PotB) stator genes are shown as motility controls at the top of each square petri dish, each supplemented with 85 mM NaCl (left) or 85 mM KCl (right). (B) Rotation speed of single tethered cells expressing PotDα and PomA variants engineered with other candidate motility-enhancing mutations detected in directed evolution experiments. The first bar on the left (PomA(H116Y)PotDα genomic) indicated the construct being expressed from the chromosomal *motAB*

locus, while all other constructs were expressed from a plasmid in a *E. coli* Δ*motAB* chassis (N = 22, 0, 19, 11, 39 cells, respectively). (C) Alphafold2 model of the chimeric stator PomA(A86V/H116Y)$_5$PotDα$_2$ with A-subunits in green and B-subunits in yellow. The position of each mutation is highlighted and labelled in red or purple on the structure and in the inset.